Journal of Sound and Vibration (1999) **220**(5), 807–825
Article No. jsvi.1998.1937, available online at http://www.idealibrary.com.on IDEAL

A QUADRATIC PROGRAMMING APPROACH TO THE DESIGN OF ACTIVE–PASSIVE VIBRATION ISOLATION SYSTEMS

D. J. Leo and D. J. Inman

Department of Mechanical Engineering, Virginia Polytechnic Institute and State University, Blacksburg, VA 24061-0261, *U.S.A.*

(*Received* 12 *January* 1998, *and in final form* 21 *August* 1998)

A quadratic programming algorithm is presented for studying the design tradeoffs of active–passive vibration isolation systems. The novelty of the technique is that the optimal control problem is posed as a quadratic optimization with linear constraints. The quadratic cost function represents the mean square response of the payload acceleration and isolator stroke, and the linear constraints represent asymptotic tracking requirements and peak response constraints. Posing the problem as a quadratic optimization guarantees that a global optimal solution can be found if one exists, and the existence of an optimal solution guarantees that the vibration isolation system satisfies the specified design constraints. The utility of the technique is demonstrated on a comparison of passive vibration isolation and active–passive vibration isolation utilizing relative displacement feedback.

1. INTRODUCTION

Passive vibration isolation is a proven approach to the reduction of energy transmission between structural components. Conventional vibration isolation systems consist of mounts placed between the source of vibration and the isolated structure. Given specifications on the level and spectral content of the input disturbance, the stiffness and damping of the mount is tailored to minimize the motion of the isolated structure while keeping within the material constraints of the isolator. Traditional design methods for passive isolation systems can be found in several handbooks and textbooks on shock and vibration analysis [1–3].

A recent development in vibration isolation technology is the use of active control techniques to improve the performance of conventional isolation systems. In contrast to a conventional isolation system, an active isolation system consists of sensors, actuators, and control electronics that reduce energy transmission

0022–460X/99/100807 + 19 $30.00/0

through feedforward or feedback control. Although currently more expensive and complex than a passive approach, advances in transducer technology and control theory are making active isolation a practical alternative to passive methods for several applications [4].

Although active isolation systems can achieve better performance than their passive counterparts, they are typically implemented in conjunction with a passive isolator to take advantage of the strengths of both methods. The strength of a passive isolator is its simplicity and inherent robustness: design techniques are well established and materials are readily available for traditional isolation applications. The strength of an active isolation system is its potential for superior isolation and its ability to adapt to changes in the operating environment. For these reasons, a combination of active and passive isolation often provides the best tradeoff between broadband performance, adaptability, and robustness.

The primary benefit of active–passive vibration isolation is that it allows more design freedom than a conventional passive approach. Several of the design tradeoffs associated with isolation design do not hold for an active–passive isolation system. For example, low frequency passive isolation is severely constrained by the tradeoff between isolator stiffness and static sag. Purely passive systems typically require complex mechanical design to achieve isolation frequencies near or below 1 Hz, whereas an active–passive approach can achieve isolation frequencies of the order of 0·2 Hz. One method of achieving low frequency isolation is to combine a stiff passive isolator in series with an active mount. The stiff passive isolator minimizes static sag and provides isolation at frequencies well above resonance, while the active mount provides isolation at low frequencies without reducing the static stiffness of the mount. Thus, combining active and passive methods provides superior performance without the complications that occur with a purely passive approach.

The use of active control technology has introduced new tradeoffs into the design of vibration isolation systems. The combination of active and passive control enables more design freedom in trading off key performance specifications such as peak payload acceleration and peak isolator stroke. In a passive isolation system, for example, minimizing the mean square acceleration of the payload constraint the peak value of the response, making it impossible to trade off these two performance specifications. Active isolation eliminates this constraint between the two performance specifications and enables peak values to be traded off against mean square responses.

The tradeoffs associated with active–passive vibration isolation have directed researchers towards the use of optimal control techniques for isolator design. Tanaka and Kikushima [5] used parameter optimization techniques for active vibration isolation design and derived a necessary set of optimality conditions. They also developed an iterative quasi Newton algorithm for solving the optimization problem. Parameter optimization techniques were also developed by Cunningham [6] and, more recently, by Sciulli and Inman [7] for understanding design tradeoffs. State space optimal control techniques were investigated by Hyde and Crawley [8] and experimentally implemented by Hyde [9]. Their work

concentrated on the use of H_2 synthesis techniques for the design of multiaxis isolation systems.

The objective of this work is to develop an efficient numerical technique for studying the tradeoffs in active–passive isolator design. The novelty of the technique is that the problem is posed as a quadratic programming problem with linear constraints. Posing the problem as a quadratic optimization guarantees that the global optimum can be found if a feasible solution exists, thus enabling design tradeoffs to be studied using a series of numerical optimizations. Furthermore, the global solution is determined without regard to the actual implementation of the device, enabling a one-to-one comparison between active–passive and purely passive isolation systems. In contrast to H_2 optimal control techniques studied by Hyde, this method also enables the explicit tradeoff of peak response specifications with mean square response specifications.

The technique is based upon work performed by Boyd and Barratt [10] in the field of convex optimization techniques for linear control design. In a previous book, Boyd and Barratt developed a general framework for posing linear control problems as convex and quasi convex optimization problems. They demonstrated that many types of practical design tradeoffs for linear control, such as peak response constraints and mean square responses, could be placed within the framework of convex optimization and solved efficiently using numerical search techniques.

The present work applies the convex optimization approach to the study of design tradeoffs for single axis active–passive vibration isolation. Three types of isolation systems will be studied: an isolation system modelled as a spring and a dashpot in parallel, a ''three-parameter'' isolator that is modelled as a spring in parallel with a series spring and dashpot, and an active–passive isolator that uses relative displacement as the sensor signal for a feedback control law (see Figure 1). These three isolators model a wide range of elastic, elastomeric, viscoelastic, and fluid mounts for vibration isolation.

The paper is divided into four sections. Models for the three isolators are stated in the first section and normalized so that they can be directly compared to the optimal active–passive designs. The second section focuses on the development of the quadratic programming approach to studying active–passive design tradeoffs. The third section is a numerical study that highlights the utility of the optimization

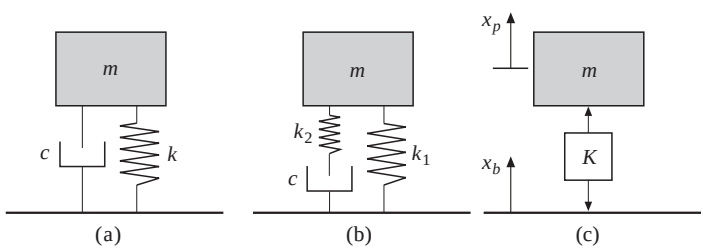

Figure 1. Isolation systems studied in this work: (a) a parallel spring and dashpot arrangement, (b) a spring in parallel with a series spring and dashpot, and (c) an active–passive isolation system.

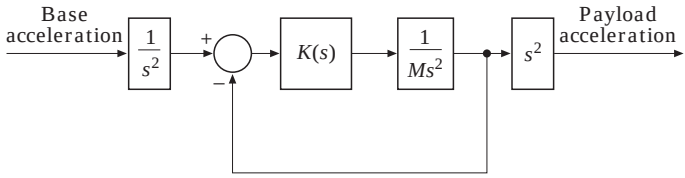

Figure 2. Block diagram of the vibration isolation control system.

technique, and the final section summarizes the work and states the main conclusions.

2. ISOLATOR MODELS AND CONTROL FORMULATION

Figure 2 is a block diagram of the single axis isolation control system. The disturbance input is the base acceleration and the isolator is designed to tailor the transmissibility between the base and the rigid payload. The relative displacement between the base and the payload is denoted δ and its Laplace transform is denoted $\Delta(s)$. For the active–passive vibration isolation system, the Laplace transform of the applied force is

$$F_{ap}(s) = K(s)\Delta(s), \tag{1}$$

where $K(s)$ is a function of the linear control law. This control law assumes that the feedback signal is simply the relative displacement between the base and the payload. Although this model does not encompass all types of active isolation systems, it does encompass many practical systems and it allows one to directly compare passive isolators with a specific type of active system. For the "three parameter" model of the passive isolator,

$$F_{tp}(s) = [(k_1 + k_2)cs + k_1k_2]/(cs + k_2)\Delta(s), \tag{2}$$

where k_1, k_2, and c are the spring and damping coefficients of the isolation system. Finally, the force applied by a pure spring and dashpot is equivalent to

$$F_p(s) = (cs + k)\Delta(s). \tag{3}$$

The spring and dashpot constants for the spring and dashpot isolator are denoted k and c, respectively. Comparing equations (2) and (3), one sees that as $k_2 \to \infty$, the ratios k_1/k_2 and c/k_2 approach zero and equation (2) reduces to equation (3). This simple analysis demonstrates that a pure spring–dashpot isolator is simply a subset of a three-parameter isolator, enabling one to limit the analysis to a comparison of active–passive control and a general three-parameter model of a passive isolator.

The pertinent design variables are the transfer function between the base acceleration and payload acceleration and the transfer function between base acceleration and actuator stroke. The block diagram shown in Figure 2 can be

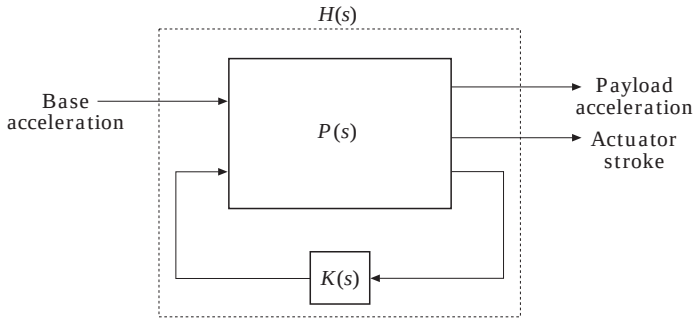

Figure 3. Standard block diagram of the multi-input-multi-output control system.

placed into the standard form of a multiinput–multioutput linear control system (see Figure 3 for block diagram) by defining

$$z = \begin{bmatrix} \ddot{x}_p \\ \delta \end{bmatrix}, \qquad w = \ddot{x}_b, \qquad y = \delta, \qquad u = f, \tag{4}$$

where $\ddot{x}_b$ is the base acceleration, $\ddot{x}_p$ is the payload acceleration, and f is the applied force. With these variable definitions, one can transform the system into the Laplace domain and write the partitions of the open loop block diagram:

$$P_{zw}(s) = \begin{bmatrix} 0 \\ 1/s^2 \end{bmatrix}, \qquad P_{yw}(s) = 1/s^2, \qquad P_{zu}(s) = \begin{bmatrix} 1/M \\ -1/Ms^2 \end{bmatrix},$$

$$P_{yu}(s) = -1/Ms^2. \tag{5}$$

Using the Q parameterization of the closed loop system, $H(s)$ [10]:

$$H(s) = P_{zw}(s) + P_{zu}(s)Q(s)P_{yw}(s), \tag{6}$$

where $Q(s) = (1/Ms^2)K(s)(I - P_{yu}(s)K(s))^{-1}$, one can express the closed loop system as a matrix function of the open loop partitions:

$$H(s) = \begin{bmatrix} 0 \\ 1/s^2 \end{bmatrix} + \begin{bmatrix} 1 \\ -1/s^2 \end{bmatrix} Q(s) \tag{7}$$

or,

$$H(s) = \begin{bmatrix} Q(s) \\ (1/s^2)(1 - Q(s)) \end{bmatrix}. \tag{8}$$

One denotes the Laplace transforms of the base acceleration, payload acceleration and actuator stroke as $A_b(s)$, $A_p(s)$, and $\Delta(s)$, respectively. With this notation, the two transfer functions of interest are

$$H_{11}(s) = A_p(s)/A_b(s) = Q(s), \qquad H_{21}(s) = \Delta(s)/A_b(s) = (1/s^2)(1 - Q(s)). \tag{9}$$

Equation (9) illustrates that the two transfer functions of interest are affine with respect to the free parameter $Q(s)$.

Equation (9) represents the result for a general linear control system. For a passive isolator modelled by equation (2), one can substitute in the expression for the applied force and determine the closed loop transfer functions in terms of the isolation parameters:

$$H_{p11}(s) = \frac{(k_1/k_2 + 1)2\zeta\omega_n s + \omega_n^2}{(2\zeta/\omega_n)(k_1/k_2)s^3 + s^2 + (k_1/k_2 + 1)2\zeta\omega_n s + \omega_n^2},$$

$$H_{p21}(s) = (1/\omega_n^2)\frac{(2\zeta\omega_n k_1/k_2)s + \omega_n^2}{2\zeta/\omega_n(k_1/k_2)s^3 + s^2 + (k_1/k_2 + 1)2\zeta\omega_n s + \omega_n^2}. \tag{10}$$

The break frequency of the isolation system, ω_n, is defined as $\sqrt{k_1/m}$ and the definition $2\zeta\omega_n = c/m$ has also been substituted into equation (10). Again, note that as $k_1/k_2 \to 0$ the transfer functions reduce to those of a pure spring and dashpot isolator.

3. PERFORMANCE SPECIFICATIONS

The first step in the control analysis is to express the physical performance specifications in terms of the closed-loop transfer functions, $H_{11}(s)$ and $H_{21}(s)$. Three sets of performance specifications will be considered for both the actuator stroke and the payload acceleration: (1) the DC value for a constant base acceleration, (2) the maximum value for a step input acceleration to the base and (3) the root mean square response to a bandlimited random noise input to the base.

Each of these specifications will be discussed in the following sections.

3.1. STEADY STATE RESPONSE TO A STEP DISTURBANCE

An isolation system is typically designed such that the relative acceleration between the payload and the base is equal to zero for a constant base acceleration. This performance specification is equivalent to the following constraint on the closed loop transfer matrix:

$$H_{11}(0) = 1. \tag{11}$$

Examining equation (9), one sees that this constraint on $H(s)$ is equivalent to the constraint on $Q(s)$:

$$Q(0) = 1. \tag{12}$$

Satisfying this expression ensures that the transmissibility is equal to 1 at $s = 0$.

3.2. FINITE ACTUATOR STROKE FOR CONSTANT BASE ACCELERATION

The second steady state performance specification ensures that the isolation system responds with a finite payload acceleration for a constant, bounded, base

acceleration. The corresponding performance specification on the closed loop transfer function matrix $H_{21}(s)$ is

$$\lim_{s\to 0} H_{21}(s) = \alpha_{dc\text{-}stroke}, \tag{13}$$

where $\alpha_{dc\text{-}stroke}$ is a finite scalar value. In terms of the free parameter $Q(s)$, this constraint is

$$\lim_{s\to 0} (1 - Q(s))1/s^2 = \alpha_{dc\text{-}stroke}. \tag{14}$$

Specifying a finite value for $H_{21}(s)$ as s approaches zero is equivalent to requiring that the term $1 - Q(s)$ have two free integrators in its numerator.

3.3. PEAK PAYLOAD ACCELERATION AND PEAK ACTUATOR STROKE TO A UNITY STEP INPUT

The second set of design specifications constrain the peak actuator stroke and peak payload acceleration for a constant base acceleration. The time response of the payload acceleration and actuator stroke to a unity step input can be written in terms of the impulse response functions:

$$z_1(t) = \int_0^t h_{11}(\tau)\,\mathrm{d}\tau, \qquad z_2(t) = \int_0^t h_{21}(\tau)\,\mathrm{d}\tau, \tag{15}$$

where $h_{11}(t)$ and $h_{21}(t)$ are the inverse Laplace transforms of the transfer functions $H_{11}(s)$ and $H_{21}(s)$. Assuming that the DC values of the actuator stroke and payload acceleration are $\alpha_{dc\text{-}stroke}$ and 1, respectively, the maximum values can be written

$$\max(z_1(t)) = 1 + \alpha_{os\text{-}acc} \max(z_2(t)) = \alpha_{dc\text{-}stroke}(1 + \alpha_{os\text{-}stroke}), \tag{16}$$

where $\alpha_{os\text{-}acc}$ and $\alpha_{os\text{-}stroke}$ represent the overshoot of the payload acceleration and actuator stroke. The constraint on the peak acceleration is defined

$$\max(z_1(t)) < 1 + \alpha_{os\text{-}acc} \max(z_2(t)) < \alpha_{dc\text{-}stroke}(1 + \alpha_{os\text{-}stroke}) \tag{17}$$

in terms of the DC value of the actuator stroke and the overshoot of the payload acceleration and isolator.

3.4. MEAN SQUARE REGULATION

One of the primary performance specifications on the isolation system is the reduction of mean square payload acceleration for a random base acceleration. The properties of the base acceleration is specified in terms of a power spectral density function, $G_w(f)$, where f is the frequency in cycles/s, and the following expression is used to compute the expected value of the response variable to the input:

$$\langle z \rangle^2 = \int_0^{f_{\max}} \|H(f)\|^2 G_w(f)\,\mathrm{d}f, \tag{18}$$

where $\|H(f)\|$ is the magnitude of the frequency response between the base acceleration and the response variable and $\langle\,\rangle^2$ denotes the mean square value of the variable. The mean square value is computed between zero frequency and the maximum frequency over which the power spectral density is defined, and it is assumed that the power spectral density is normalized such that its integral is equal to the mean square value of the input [11], i.e.,

$$\langle w\rangle^2 = \int_0^{f_{\max}} G_w(f)\,\mathrm{d}f. \tag{19}$$

For the present problem, the relevant design variables are the payload acceleration and actuator stroke, therefore the mean square value of the response variables are expressed by the functions

$$\langle z_1\rangle^2 = \int_0^{f_{\max}} \|H_{11}(f)\|^2 G_w(f)\,\mathrm{d}f, \qquad \langle z_2\rangle^2 = \int_0^{f_{\max}} \|H_{21}(f)\|^2 G_w(f)\,\mathrm{d}f. \tag{20}$$

Substituting the expressions for the closed loop transfer functions, equation (9), into the previous expression yields the mean square performance specifications as a function of the free parameter, $Q(s)$:

$$\langle z_1\rangle^2 = \int_0^{f_{\max}} \|Q(f)\|^2 G_w(f)\,\mathrm{d}f, \qquad \langle z_2\rangle^2 = \frac{1}{16\pi^4}\int_0^{f_{\max}} \left\|(1 - Q(f))\,\frac{1}{f^2}\right\|^2 G_w(f)\,\mathrm{d}f. \tag{21}$$

These two expressions will be used for the numerical control optimizations.

4. FINITE DIMENSIONAL PARAMETERIZATION OF THE CLOSED-LOOP SYSTEM

The performance specifications and constraint equations can be expressed as a finite dimensional expression by substituting the expansion

$$Q(s) = \sum_{i=1}^{N} x_i Q_i(s) \tag{22}$$

for the free parameters. The functions $Q_i(s)$ are specified, N is the number of terms in the expansion, and the scalar variables x_i are the design variables for the control optimization. For the present analysis, the following parameterization of the closed loop system will be used:

$$Q_i(s) = (1/[s + \omega_n])^i, \tag{23}$$

where, by the definition of $H_{11}(s)$, the parameter ω_n is the break frequency of the isolation system. The parameterization is normalized with respect to the break frequency of the isolation system by substituting

$$s = \omega_n \sigma \tag{24}$$

into equation (23). Combining equations (22) through (24) yields

$$Q(\sigma) = \sum_{i=1}^{N} \frac{x_i}{\omega_n^i} \left(\frac{1}{\sigma + 1} \right)^i. \tag{25}$$

Substituting $\xi_i = x_i/\omega_n^i$ into equation (25) yields the nondimensional parameterization

$$Q(\sigma) = \sum_{i=1}^{N} \xi_i \left(\frac{1}{\sigma + 1} \right)^i. \tag{26}$$

The non-dimensional parameterization, equation (26), is used to write $H_{11}(s)$ and $H_{21}(s)$ as a function of the non-dimensional frequency, σ:

$$H_{11}(\sigma) = Q(\sigma) = \sum_{i=1}^{N} \xi_i \left(\frac{1}{\sigma + 1} \right)^i,$$

$$H_{21}(\sigma) = \frac{1}{\omega_n^2 \sigma^2} (1 - Q(\sigma)) = \frac{1}{\omega_n^2 \sigma^2} \left(1 - \sum_{i=1}^{N} \xi_i \left(\frac{1}{\sigma + 1} \right)^i \right). \tag{27}$$

These two expressions will be the basis for the quadratic optimization procedures described in the following sections.

4.1. ASYMPTOTIC TRACKING

Using the finite dimensional expansions of the closed loop systems, equation (27), enables the two transfer functions of interest to be written as

$$H_{11}(\sigma) = \frac{a_1 \sigma^{N-1} + a_2 \sigma^{N-2} + \cdots + a_{N-1}\sigma + a_N}{\sigma^N + b_1 \sigma^{N-1} + \cdots + b_{N-1}\sigma + b_N},$$

$$H_{21}(\sigma) = \frac{\sigma^N + (b_1 - a_1)\sigma^{N-1} + \cdots + (b_{N-1} - a_{N-1})\sigma + (b_N - a_N)}{\omega_n^2 \sigma^2 (\sigma^N + b_1 \sigma^{N-1} + \cdots + b_{N-1}\sigma + b_N)}, \tag{28}$$

where the scalar functions a_i, $i = 1, \ldots, N$, are functions of the design variables ξ_1. Satisfying the two DC constraints yields the following three equations:

$$b_{N-2} - a_{N-2} = \omega_n^2 b_N \alpha_{dc\text{-}stroke}, \qquad b_{N-1} - a_{N-1} = 0, \qquad b_N - a_N = 0. \tag{29}$$

Since the scalar variables a_i are linear functions of the design variables, these three equations are linear constraints on ξ:

$$F\xi + G = 0. \tag{30}$$

The matrices $F \in \Re^{3 \times N}$ and $G \in \Re^3$ are real-valued matrices whose coefficients vary as the number of terms in the finite dimensional approximation to $H(\sigma)$ is increased.

4.2. PEAK PAYLOAD ACCELERATION AND PEAK ACTUATOR STROKE

The peak values of the actuator and payload acceleration can be written as a linear constraint on the design variables, ξ_i. With the parameterization defined by equation (23), the time response of the payload acceleration can be written in terms of the inverse Laplace transform of $Q_i(\sigma)$:

$$z_1(\tau) = \sum_{i=1}^{N} \frac{\xi_i}{(i-1)!} \int_0^{\tau} \theta^{i-1} \, \mathrm{e}^{-\theta} \, \mathrm{d}\theta, \tag{31}$$

where τ is a non-dimensional variable, $\tau = \omega_n t$. To satisfy the constraint equation

$$z_1(\tau) < 1 + \alpha_{os\text{-}acc}, \tag{32}$$

the following expression must be satisfied:

$$\sum_{i=1}^{N} \frac{\xi_i}{(i-1)!} \int_0^{\tau} \theta^{i-1} \, \mathrm{e}^{-\theta} \, \mathrm{d}\theta < 1 + \alpha_{os\text{-}acc}, \tag{33}$$

which can be rewritten as the linear matrix expression

$$D_{pk\text{-}acc}\xi + E_{pk\text{-}acc} < 0 \tag{34}$$

by discretizing τ. The matrices of equation (33) are defined by the expressions

$$(D_{pk\text{-}acc})_{ji} = \frac{1}{(i-1)!} \int_0^{\tau_j} \theta^{i-1} \, \mathrm{e}^{-\theta} \, \mathrm{d}\theta, \qquad (E_{pk\text{-}acc})_j = -(1 + \alpha_{os\text{-}acc}). \tag{35}$$

where τ_j is the non-dimensional time at the jth step, $j = 1, \ldots, n_\tau$.

The peak actuator constraint can be written in a similar way by examining the step response of $z_2(\tau)$:

$$z_2(\tau) = \frac{1}{2\omega_n^2} \tau^2 - \frac{1}{\omega_n^2} \sum_{i=1}^{N} \int_0^{\tau} \int_0^{\theta} \int_0^{\theta'} \frac{\xi_i}{(i-1)!} \theta''^{i-1} \, \mathrm{e}^{-\theta''} \, \mathrm{d}\theta'' \, \mathrm{d}\theta' \, \mathrm{d}\theta. \tag{36}$$

To satisfy the constraint

$$z_2(\tau) < \alpha_{dc\text{-}stroke}(1 + \alpha_{os\text{-}stroke}), \tag{37}$$

the following linear matrix expression must be satisfied:

$$D_{pk\text{-}stroke}\xi + E_{pk\text{-}stroke} < 0, \tag{38}$$

where

$$(D_{pk\text{-}stroke})_{ji} = -\int_0^{\tau_j} \int_0^{\theta} \int_0^{\theta'} \frac{1}{(i-1)!} \theta''^{i-1} \, \mathrm{e}^{-\theta''} \, \mathrm{d}\theta'' \, \mathrm{d}\theta' \, \mathrm{d}\theta,$$

$$(E_{pk\text{-}stroke})_j = \tfrac{1}{2}\tau_j^2 - \omega_n^2 \alpha_{dc\text{-}stroke}(1 + \alpha_{os\text{-}stroke}). \tag{39}$$

Equations (34) and (38) can be combined into one linear matrix expression by defining

$$D = \begin{bmatrix} D_{pk\text{-}acc} \\ D_{pk\text{-}stroke} \end{bmatrix}, \qquad E = \begin{bmatrix} E_{pk\text{-}acc} \\ E_{pk\text{-}stroke} \end{bmatrix} \tag{40}$$

and rewriting the constraint as

$$D\xi + E < 0, \tag{41}$$

which is, as expected, an affine expression in the design variables ξ_i.

4.3. MEAN SQUARE MITIGATION

The expression for the mean square values of the design variables can also be placed in matrix form. Substituting $f = f_n\sigma$ into equation (27) and normalizing the power spectral density with respect to the maximum value of $G_w(f)$, i.e., $G_w(f) = \Gamma_w G_w(\sigma)$, where Γ_w is the maximum value of the power spectral density, the expressions for the mean square response of z_1 and z_2 can be written:

$$\langle z_1 \rangle^2 = \Gamma_w f_n \int_0^{\sigma_{\max}} \|Q(\sigma)\|^2 G_w(\sigma)\, \mathrm{d}\sigma,$$

$$\langle z_2 \rangle^2 = \frac{\Gamma_w}{16\pi^4 f_n^3} \int_0^{\sigma_{\max}} \left\| (1 - Q(\sigma)) \frac{1}{\sigma^2} \right\|^2 G_w(\sigma)\, \mathrm{d}\sigma. \tag{42}$$

Rearranging terms results in two non-dimensional performance functions that define the mean square response of the payload acceleration and isolator stroke:

$$\frac{1}{\Gamma_w f_n} \langle z_1 \rangle^2 = \int_0^{\sigma_{\max}} \|Q(\sigma)\|^2 G_w(\sigma)\, \mathrm{d}\sigma,$$

$$\frac{16\pi^4 f_n^3}{\Gamma_w} \langle z_2 \rangle^2 = \int_0^{\sigma_{\max}} \left\| (1 - Q(\sigma)) \frac{1}{\sigma^2} \right\|^2 G_w(\sigma)\, \mathrm{d}\sigma. \tag{43}$$

Expanding the vector form of the finite dimensional parameterization allows one to write the expressions in equation (21) as

$$1/\Gamma_w f_n \langle z_1 \rangle^2 = \xi^{\mathrm{T}} A_{rms\text{-}acc} \xi,$$
$$16\pi^4 f_n^3/\Gamma_w \langle z_2 \rangle^2 = \xi^{\mathrm{T}} A_{rms\text{-}stroke} \xi + B_{rms\text{-}stroke}^{\mathrm{T}} \xi + c_{rms\text{-}stroke}, \tag{44}$$

where

$$(A_{rms\text{-}acc})_{ij} = \int_0^{\sigma_{\max}} [\Re(Q_i(\sigma))\Re(Q_j(\sigma)) + \Im(Q_i(\sigma))\Im(Q_j(\sigma))] S_w(\sigma)\, \mathrm{d}\sigma,$$

$$(A_{rms\text{-}stroke})_{ij} = \int_0^{\sigma_{\max}} [\Re(Q_i(\sigma))\Re(Q_j(\sigma)) + \Im(Q_i(\sigma))\Im(Q_j(\sigma))] \frac{S_w(\sigma)}{\sigma^4}\, d\sigma,$$

$$(B_{rms\text{-}stroke})_i = -\int_0^{\sigma_{\max}} \Re(Q_i(\sigma)) \frac{S_w(\sigma)}{\sigma^4}\, d\sigma, \qquad c_{rms\text{-}stroke} = \int_0^{\sigma_{\max}} \frac{S_w(\sigma)}{\sigma^4}\, d\sigma. \quad (45)$$

All of the terms in the previous four expressions can be evaluated numerically for the specified finite dimensional parameterization of $Q(\sigma)$.

5. QUADRATIC OPTIMIZATION

The previous sections describe a method for posing the vibration isolation and design problem as a constrained quadratic optimization of the form

$$\min \xi^T A\xi + B\xi + c, \qquad \text{s.t. } D\xi + E < 0, \qquad F\xi + G = 0. \quad (46)$$

A series of numerical analyses were performed to illustrate the use of the quadratic programming techniques for vibration isolation design. The tradeoff between mean square payload acceleration and mean square actuator stroke can be determined by solving a series of quadratic optimizations. For a specified number of terms in the finite dimensional parameterization of $Q(\sigma)$, the coefficient matrices of the cost function can be defined as

$$A = \lambda_1 A_{rms\text{-}acc} + \lambda_2 A_{rms\text{-}stroke}, \qquad B = \lambda_2 B_{rms\text{-}stroke}, \qquad c = \lambda_2 c_{rms\text{-}stroke}, \quad (47)$$

where λ_1 and λ_2 are scalar constants normalized such that

$$\lambda_1 + \lambda_2 = 1. \quad (48)$$

Varying the scalar constants varies the relative weight of the mean square acceleration and mean square actuator stroke in the cost function and enables the tradeoff curve to be plotted.

At the extreme case of $\lambda_1 = 1$, the cost function simply minimizes the mean square payload acceleration, whereas the opposite extreme ($\lambda_2 = 1$) yields a control law that minimizes the mean square actuator stroke. Several studies were performed to determine the number of terms that were required to achieve convergence of the optimal solutions. All studies indicated that 10 terms were sufficient to provide convergence of the quadratic cost function.

The optimal active–passive isolators were compared directly with the results of a parameter study of passive control. The closed loop transfer functions for a passive isolator (as shown in equation (10)) were non-dimensionalized by substituting $s = \omega_n \sigma$ and $\kappa = k_1/k_2$ into the equation, yielding the following non-dimensional expressions:

$$H_{11}(\sigma) = \frac{(\kappa + 1)2\zeta\sigma + 1}{2\zeta\kappa\sigma^3 + \sigma^2 + (\kappa + 1)2\zeta\sigma + 1},$$

$$\omega_n^2 H_{21}(\sigma) = \frac{2\zeta\kappa\sigma + 1}{2\zeta\kappa\sigma^3 + \sigma^2 + (\kappa + 1)2\zeta\sigma + 1}. \quad (49)$$

TABLE 1

Nomenclature for the tradeoff curves

Symbol	Definition
f_n (Hz)	isolator frequency
σ –	normalized frequency, f/f_n
$\langle z_1 \rangle$ (m/s^2)	root mean square payload acceleration
$\langle z_2 \rangle$ (m)	root mean square isolator stroke
Γ_w m^2/s^4/Hz	maximum value of the input spectrum
$\alpha_{os_{acc}}$ –	overshoot of the payload acceleration
$\alpha_{os_{stroke}}$ –	overshoot of the isolator stroke
κ –	relative stiffness for a three-parameter isolator ($\kappa = 0$ represents a spring–dashpot isolator)

The mean square and peak responses for passive isolation could be numerically determined by simply solving these equations for a range of damping ratios and stiffness ratios.

6. TRADEOFF STUDIES

Two sets of tradeoff studies were performed. The tradeoff studies compared passive isolation systems with active isolation systems that utilize relative displacement as the feedback signal. The first tradeoff study compared mean square mitigation without any constraints on the peak value of the payload acceleration and isolator stroke. The mean square mitigation was compared for both broadband and bandlimited random disturbances, where the disturbances were modelled with varying input power spectral densities. The second set of tradeoff studies examined mean square mitigation for active–passive isolation in the presence of increasingly stringent constraints on the isolator stroke and peak payload acceleration.

6.1. MEAN SQUARE MITIGATION FOR UNCONSTRAINED PEAK RESPONSE

A series of tradeoff studies were performed to compare mean square mitigation without any constraints on the peak response of the payload acceleration or isolator stroke (i.e., $\alpha_{os_{acc}}$ and $\alpha_{os_{stroke}} \gg 1$). The tradeoff curve for active–passive isolation was determined by solving a series of quadratic optimizations using the procedure described in the previous section. The tradeoff curve for passive isolation was determined by computing the mean square payload acceleration and mean square isolator stroke for values of ζ between 0 and 1 and $\kappa = 0$, 0·25, 0·50, 0·75, and 1·0. The nomenclature for the tradeoff curves is summarized in Table 1.

The plot on the left of Figure 4 is the tradeoff curve for the case of a broadband input disturbance. The normalized spectral content of the input is shown above the tradeoff curve. The lower curve on the plot is the tradeoff in mean square performance for the active–passive vibration isolation system. Each point on the curve represents a solution to the quadratic optimization for particular values of λ_1 and λ_2 and the region above the tradeoff curve is the feasible region for the

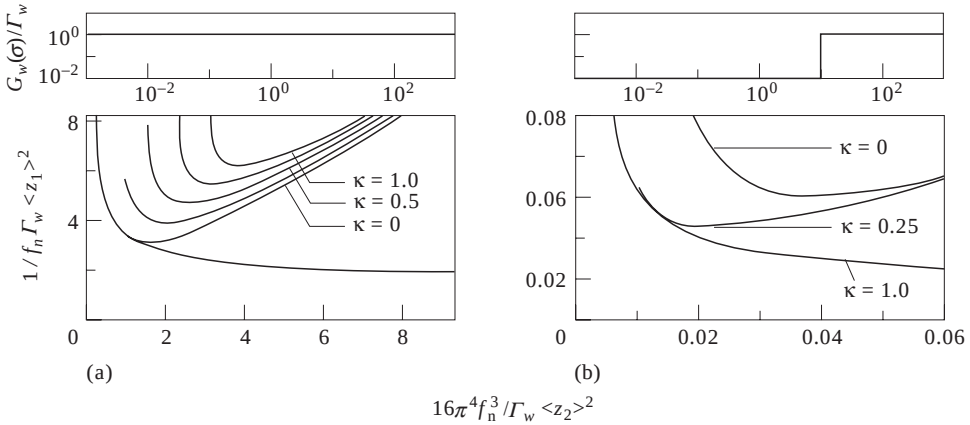

Figure 4. Tradeoff curves comparing passive isolation and active–passive isolation utilizing relative displacement feedback: (a) broadband input spectrum and (b) bandlimited input spectrum. The normalized input spectrums are displayed above the tradeoff curves.

active–passive isolation. The region below the curve represents the set of infeasible solutions, i.e., there is no active–passive isolation system that will achieve these values for mean square payload acceleration and mean square isolator stroke.

As the plot demonstrates, the mean square performance of the passive isolation system lies inside the feasible region of the active–passive isolation system. This is to be expected due to the fact that a passive compensator is simply a subset of an active–passive design. The tradeoff curve also demonstrates that, for a broadband input disturbance, a simple spring–dashpot isolation system (i.e., $\kappa = 0$) is the most effective passive isolation system; it achieves the smallest mean square payload acceleration and mean square isolator stroke of any passive isolator. This is attributed to the fact that a pure spring–dashpot isolation system can achieve higher values of damping, and thus lower resonant peaks, than the isolation system illustrated in the middle of Figure 1. The final conclusion that can be drawn from this tradeoff study is that for equivalent isolator break frequencies, an active–passive isolation system can achieve 66% greater reduction in mean square payload acceleration than a passive isolator.

The plot on the right of Figure 4 demonstrates that the performance tradeoffs are a function of the frequency content of the input disturbance. For a power spectral density function that has a significant increase in energy near the break frequency of the isolator, the active–passive design achieves approximately a factor of two greater reduction in the mean square payload acceleration than the most effective passive design studied ($\kappa = 0{\cdot}25$). Furthermore, in contrast to the tradeoff for a broadband input spectrum, a pure spring–dashpot isolator is not the most effective type of passive isolation system. As the curves for various values of κ demonstrate, a pure spring and dashpot arrangement results in significantly higher mean square payload accelerations and higher mean square strokes than several of the other types of isolators. This is attributed to the fact that the increased rolloff of the isolator for values of $\kappa > 0$ reduces the mean square response more significantly than increased damping near resonance.

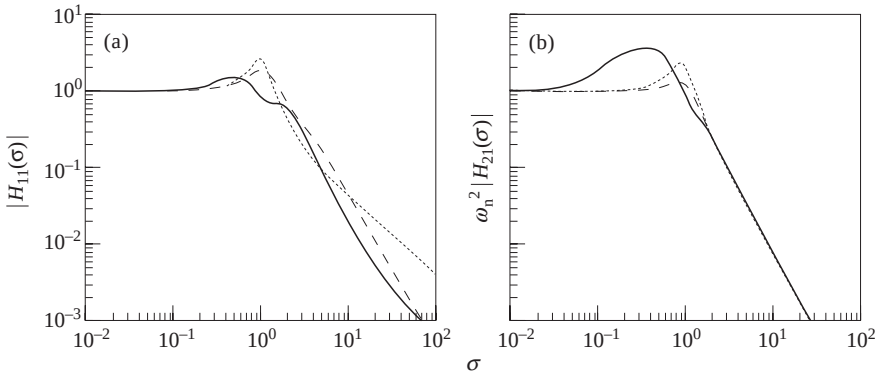

Figure 5. Normalized closed loop transfer functions for active–passive control (solid), a pure spring and dashpot isolator (short dash) and a three-parameter isolator (long dash): (a) payload acceleration/base acceleration and (b) isolator stroke/base acceleration.

The differences in the optimal results can be illustrated by examining the optimal closed loop transfer functions for the different types of isolators. Figure 5 is a plot of the closed loop transfer functions $H_{11}(\sigma)$ and $H_{21}(\sigma)$ for active–passive isolation, a pure spring–dashpot isolator ($\kappa = 0$), and a three-parameter isolator in which $\kappa = 0{\cdot}25$. All three are the optimal compensators for the bandlimited disturbance shown on the right of Figure 4. The poor performance of the spring–dashpot isolator is attributed to the high frequency rolloff of the transfer function $H_{11}(\sigma)$. The fact that the high frequency rolloff is constrained to be a slope of 20 dB/decade at high frequencies increases the mean square value of the payload acceleration.

The three-parameter isolator ($\kappa = 0{\cdot}25$) is able to achieve better mean square mitigation due to the fact that it rolls off with a slope of 40 dB/decade above resonance. The active–passive isolation system achieves the best reduction in mean square acceleration by increasing the damping near the isolator resonance—as

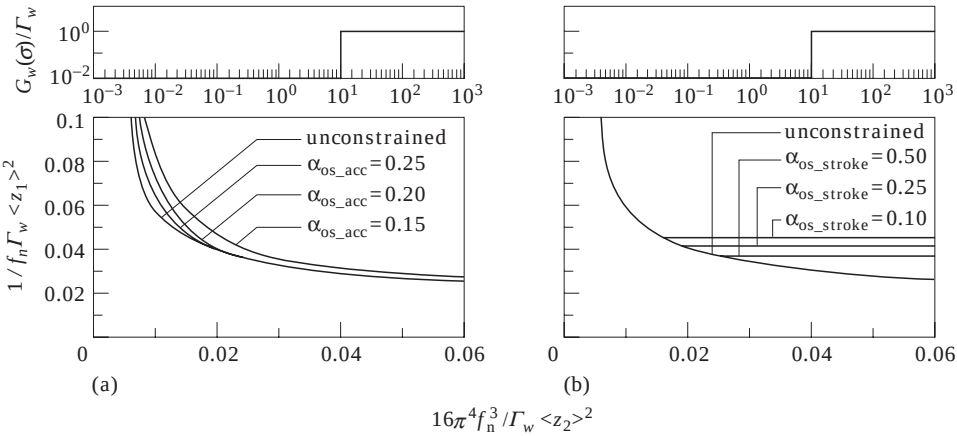

Figure 6. Tradeoff curves for a bandlimited input spectrum with hard constraints on the stroke and acceleration: (a) peak acceleration constraints, and (b) peak constraints on the isolator stroke. The active control law utilizes relative displacement as the feedback signal.

exhibited by its lower peak value—and rolling off with a slope slightly greater than 40 dB/decade above resonance.

6.2. MEAN SQUARE MITIGATION FOR CONSTRAINED PEAK RESPONSE

A separate set of tradeoff studies were performed for the case of constrained peak accelerations and constrained isolator strokes. Figure 6 is a plot of the tradeoff curves for two sets of quadratic optimizations. The plot on the left represents a series of tradeoff curves for the case of increasingly tight constraints on the peak payload acceleration but without any constraint on the peak isolator stroke. The plot on the right illustrates the tradeoff for increasingly tight constraints on the peak isolator stroke but no constraint on the peak payload acceleration.

The results indicate that the two constraints yield significantly different design tradeoffs for mean square mitigation. Constraining the overshoot of the payload acceleration between 15% and 25% does not significantly reduce the achievable performance of active–passive isolation system. This is indicated on the tradeoff curve by the fact that the maximum achievable reduction in the mean square value of z_1 is not appreciably affected when $\alpha_{os\text{-}acc}$ is between 0·15 and 0·25. In contrast, the tradeoff curve on the right of Figure 6 indicates that constraining the peak value of the isolator stroke has a significant affect on the maximum achievable reduction in the mean square acceleration. With no constraint on the peak acceleration, the minimum value of $\langle z_1\rangle^2/f_n\Gamma_w \approx 0{\cdot}025$, whereas the value increases to $\approx 0{\cdot}045$ when the peak isolator stroke is constrained to be only 10% of the static value.

6.2.1. *Numerical example*

A numerical example illustrates the use of the tradeoff curves obtained from the convex optimizations. If one assumes that the power spectral density of the base acceleration is modelled by the function

$$G_w(f) = \begin{Bmatrix} 10^{-6}\,\boldsymbol{g}^2/\text{Hz}, & 0{\cdot}005 < f < 50\ \text{Hz}, \\ 10^{-4}\,\boldsymbol{g}^2/\text{Hz}, & 50 < f < 5000\ \text{Hz}, \end{Bmatrix} \tag{50}$$

TABLE 2

Numerical results for a particular input disturbance and isolator frequency ($f_n = 5$ Hz and $\Gamma_w = 0{\cdot}00962\ m^2/s^4/Hz$)

	Fig. 4(b)			Fig. 6(b)
	$\kappa = 0$	$\kappa = 0{\cdot}25$	a-p	a-p
$\langle z_1\rangle^2/f_n\Gamma_w$	0·061	0·047	0·025	0·045
$16\pi^4 f_n^3/\Gamma_w\langle z_2\rangle^2$	0·038	0·022	0·050	0·015
$\langle z_1\rangle$ (m/s^2)	0·052	0·0476	0·0347	0·0465
$\langle z_1\rangle$ (m$\boldsymbol{g}$)	5·53	4·85	3·54	4·74
$\langle z_2\rangle$ (μm)	43·3	33·0	49·7	27·2

and that the isolator frequency is chosen to be 5 Hz, then the normalized power spectral density is equivalent to those shown in Figure 4(b) and Figure 6. Integrating the power spectral density over this frequency range yields a root mean square base acceleration of approximately 0·70 $\boldsymbol{g}$, or 6·87 m/s^2. The peak value of the power spectral density, Γ_w, is equal to 0·0001 $\boldsymbol{g}^2$/Hz, or 0·00962 m^2/s^4/Hz. The values f_n and Γ_w are the only parameters required to compute the root mean square payload acceleration and isolator stroke.

Figure 4(b) is applicable if there are no constraints on the peak payload acceleration or the peak isolator stroke. Table 2 lists the minimum value of $\langle z_1 \rangle^2 / f_n \Gamma_w$ for the passive and active–passive isolators. The root mean square payload acceleration and root mean square isolator stroke are computed from the non-dimensional quantities and are listed at the bottom of the table. The results indicate that a pure spring–dashpot isolator results in a root mean square acceleration of 5·53 m$\boldsymbol{g}$ for an isolator stroke of 43·5 μm. A more effective passive isolation system is a three-parameter isolator with a stiffness ratio of 0·25. This type of design would reduce the root mean square payload acceleration to 4·85 m$\boldsymbol{g}$ and would only require 33·3 μm of stroke. The most effective isolation system is an active–passive design, which achieves a root mean square payload acceleration of only 3·54 m$\boldsymbol{g}$, but requires almost 50 μm of isolator stroke. Furthermore, the active–passive isolators represent the limits of performance for any active control system that utilizes relative displacement as the feedback signal.

Figure 6(b) is applicable if there are hard constraints on the maximum value of the isolator stroke. Assuming that the base acceleration is a 1 $\boldsymbol{g}$ step input, the static stroke of the isolator is equivalent to $9{\cdot}81/(5^2 \times 4\pi^2)$ m, or approximately 1 cm. Constraining the isolator to less than 1·1 cm of stroke is equivalent to setting $\alpha_{os_{stroke}} = 0{\cdot}1$. The results for this case are listed in the rightmost column of Table 2. The results indicate that the hard constraint on the isolator stroke increases the root mean square payload acceleration from 3·54 m$\boldsymbol{g}$ to 4·74 m$\boldsymbol{g}$ (a 35% performance drop) and reduces the stroke from approximately 50 μm to 27 μm. The isolator performance with a hard constraint on the maximum stroke is roughly equivalent to a three-parameter isolator with a stiffness ratio of 0·25.

The numerical analyses demonstrate the utility of the quadratic optimization approach to the design of active–passive isolation systems. Several practical tradeoffs were studied using the general framework developed in this paper, including the tradeoff in mean square acceleration versus mean square isolator stroke, the effect of peak constraints on the achievable performance, and the direct comparison of an active–passive design with traditional passive isolation techniques. Although the numerical analyses presented in this paper were for a particular set of input disturbances and design constraints, the technique is useful for any type of comparison between active–passive and passive isolation.

7. CONCLUSIONS

A unified approach to the design of active–passive isolation systems was developed. The approach was based on a quadratic programming algorithm that accounted for the tradeoffs between mean square response mitigation and peak

response constraints. The quadratic programming algorithm was developed through the Q parameterization of the closed loop transfer functions. Parameterizing the closed loop transfer functions in this manner enabled the optimal control problem to be posed as a quadratic minimization with linear equality and inequality constraints. The quadratic functions represented the mean square performance specifications and the linear constraints represented the asymptotic tracking requirements and peak response constraints.

The optimal control problem was normalized so that a class of active–passive isolation designs could be studied by solving a series of numerical optimizations. For a particular input disturbance modelled by a power spectral density function, the tradeoff between mean square performance requirements was solved by performing a series of quadratic optimizations. Constraints on the peak response of the payload and peak response of the isolator stroke could be included in the analysis and another series of optimizations performed to determine the effect of the additional requirements.

The utility of the technique was demonstrated for a class of input disturbances and for a specific type of active control law. Active control systems utilizing relative displacement feedback were compared to passive systems modelled as springs and dashpots. The series of optimizations demonstrated that the design tradeoffs were significantly affected by the shape of the input spectral density and the value of the peak response constraints. The optimal active–passive isolation system was compared directly with a purely passive approach to determine the maximum amount of improvement that could be achieved with an active design. The numerical studies indicated that the performance advantage gained by implementing an active control system also varied significantly with the energy content of the input disturbance. For the disturbance cases studied, the optimal control technique demonstrated that active–passive control has significant advantages over passive control when the input energy shows a large increase near the break frequency of the isolation system.

REFERENCES

1. L. L. Beranek and I. L. Ver 1992 *Noise and Vibration Control Engineering*. New York: Wiley-Interscience.
2. C. M. Harris (editor) 1988 *Shock and Vibration Handbook*. New York: McGraw Hill.
3. D. J. Inman 1994 *Engineering Vibration*. Englewood Cliffs: Prentice-Hall.
4. A. Beard, D. Flotow and A. Flotow 1994 In *Proceedings of the SPIE International Society for Optimal Engineering* **2264**, 38–49. Practical product implementation of an active–passive vibration system.
5. N. Tanaka and Y. Kikushima 1988 *Journal of Vibration and Acoustics* **110**, 42–48. Optimal design of active vibration isolation system.
6. D. Cunningham 1993 In *Proceedings of Damping* '93, **2**. Performance/sizing tradeoffs in active and passive launch isolation.
7. D. Sciulli and D. Inman 1996 In *Proceedings of the SPIE—The International Society for Optimal Engineering* **2720**, 293–304. Comparison of single- and two-degree-of-freedom models for passive and active vibration isolation.
8. T. T. Hyde and E. Crawley 1995 In *Proceedings of the American Control Conference* **5**, 3835–3839. H_2 synthesis for active vibration isolation.

9. T. T. HYDE 1997 In *Proceedings of the Structures, Structural Dynamics and Materials Conference* **2**, 1763–1773. Experimental study of active vibration isolation.
10. S. BOYD and C. BARRATT 1991 *Linear Controller Design: Limits of Performance*. Englewood Cliffs: Prentice-Hall.
11. J. BENDAT and A. PIERSOL 1966 *Measurement and Analysis of Random Data*. New York: John Wiley.